Tribological properties of dispersions based on reduced graphene oxide sheets and trimethylolpropane trioleate or PAO 40 oils

José M. Liñeira del Río[a], Enriqueta R. López[a], Josefa Fernández[a,*], Fátima García[b]

[a]Laboratory of Thermophysical Properties, Nafomat Group, Department of Applied Physics, Faculty of Physics, University of Santiago de Compostela, 15782, Santiago de Compostela, Spain

[b]Centro de Investigación en Química Biolóxica e Materiais Moleculares (CIQUS) and Departamento de Química Orgánica, Universidade de Santiago de Compostela, 15782 Santiago de Compostela, Spain

*Corresponding author.

E-mail address: josefa.fernandez@usc.es (J. Fernandez)

Abstract

The main goal of this work is to study the tribological properties of nanolubricants formed by trimethylolpropane trioleate (TMPTO) or a polyalphaolefin (PAO 40) base oils with reduced graphene oxide sheets (rGO). This reduction was carried out in order to have a good stability of the nanoadditives in the fluids. For this aim, rGO nanopowders were prepared by thermal reduction of graphene oxide (GO) powders using KOH/ethanol as reducing agent. Tribological behavior of nanolubricants based on TMPTO and on PAO 40 oils with 0.05, 0.10, 0.25 and 0.50 wt% of rGO was evaluated. The tribological tests were carried out with a tribometer operating in ball on disk configuration and rotational mode under a working load of 20 N at room temperature. In order to analyze the wear track through the width, depth and cross-section area of the scar, a 3D optical profilometer was used. The best antifriction performance was found for 0.25 wt% rGO nanodispersions, with a 24% and a 20% enhancement for the PAO 40 and the TMPTO base oils, respectively. Moreover, for this last nanodispersion, a reduction of 24 % in the wear track width was obtained.

Keywords: reduced graphene oxide; nanolubricants; friction; wear

1. Introduction

Nanotechnology is considered the key technology of the 21st century. Among the fields of application of this technology, recent investigations have proven that the addition of different nanostructures to lubricants is effective for the reduction of wear and friction in mechanical systems [1,2]. Thus, many different kinds of nanomaterials appeared with interesting antifriction and antiwear properties, specifically nanolubricants based on graphene-type structures [3,4]. Graphitic materials have been extensively explored as additives of lubricant in oils or greases to improve their tribological properties, showing reduced friction capacity and antiwear properties in comparison with other nanoadditives [5-7] and employed to enhance the thermal conductivities of lubrication systems. Graphene materials are carbon nanostructures consisting in a single layer of carbon packed in a hexagonal lattice, with a carbon-carbon distance of 0.142 nm in a unique atom-thick 2D structure, with amazing mechanical and thermal properties, big specific surface area and good chemical stability [8,9]. Nowadays a variety of graphene-based lubricant oil additives has been and is being investigated, such us ultrathin graphene [9,10], alkylated graphene [11,12], reduced graphene oxide [13-16], chemically functionalized reduced graphene oxide [7,17] or graphene oxide monolayer [18,19].

Studies on the enhancement of the antifriction and antiwear properties due to the effect of dispersing rGOs on lubricant oils have been previously reported [13,15,16]. Schlüter et al. [16] determined the Stribeck curves of two nanodispersions composed by an additivated and fully saturated ester oil and thermally reduced graphite oxide flakes (Oxygen content of 14 wt%) finding better lubricating properties with respect to those of the base oil. Li et al. [15] measured the tribological properties of dispersions of a polyalphaolephin (PAO6) containing different kinds of rGOs (Oxygen contents between 8.1 and 11.7 wt%) concluding that the wear and friction behavior strongly depends on the synthetic procedure. Gupta et al. [13] found that for rGO dispersions in a polyalkylene (PEG) oil for low and high rGO concentrations the friction and wear are worse than for the base oil, whereas for intermediate concentrations these properties are

strongly improved. In all these studies [13-16] graphite was used as starting material for the rGO synthesis and tribological measurements were evaluated in only one lubricant.

In this work, reduced graphene oxide sheets (rGO) with lower Oxygen content (7%) have been synthesized by using commercial graphene oxide as starting material instead of graphite. The synthesized rGO has a big specific surface area and its tribological behaviour as additive for two lubricant bases of different nature have been tested under the same working conditions in order to determine its effect in the wear and friction depending on the base type. The first one, a polyester lubricant oil (trimethylolpropane trioleate, TMPTO) is a non-fully saturated ester synthetized from the oleic fatty acid and trimethylolpropane. This nonflammable ester has excellent lubricant properties and biodegradability above the 80% [20-22]. PAOs are composed by saturated oligomers manufactured *via* the catalytic oligomerisation of alphaolefins [23]. Specifically, PAO 40 is a high viscosity PAO, which is mainly used as high-performance functional base fluid in several industrial and automotive applications as gear oil, compressor oil, hydraulic fluid, grease and engine oil [24].

One of the main problems that are found when working with nanolubricants is their sedimentation stability. In the present work detailed stability studies were carried out. These studies involve: visual control of the dispersions of GO and rGO during 240 h after the dispersion preparation, refractometry measurements for the same dispersions (45 h) and dynamic light scattering (DLS) over 150 h in order to monitor the variation of the apparent average particle size and therefore assess its sedimentation.

2. Experimental section

2.1. Materials

The TMPTO base oil was kindly provided by Croda and PAO 40 was supplied by REPSOL. An aliquot of the first one has been fully characterized in a previous contribution [25]. Among the different techniques employed to characterize the TMPTO sample, we have used high performance liquid chromatography. This technique showed that this oil is composed by 68.3 %

of trimethylolpropane trioleate, 27.6 % of a compound with a C=C bond more than TMPTO (i.e. two H atoms less) and 4.1 % of a compound with two extra C=C bonds (i.e. four H atoms less) [25]. The Fourier Transform infrared spectrum (FTIR) of the TMPTO oil is shown in Fig. 1. This oil has a density at 313.15 K of 0.9037 g·cm^{-3}, a kinematic viscosity of 48.5 cSt at the same temperature and its viscosity index is 190 [25].

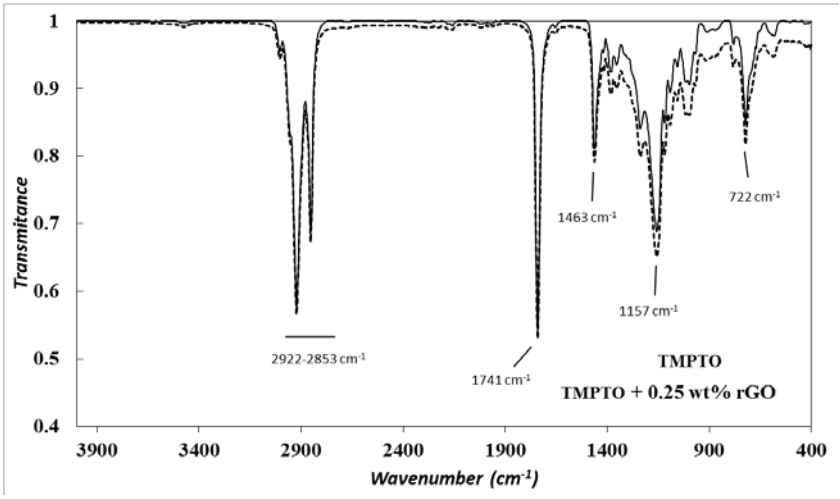

Fig. 1. FTIR spectra of TMPTO (-) and 0.25 wt% rGO nanodispersion (--).

The polyalphaolephin PAO 40 is obtained by the polymerization of 1-decene followed by hydrogenation. The PAO 40 used in this work has a density at 313.15 K of 0.8346 g·cm^{-3}, a kinematic viscosity at 313.15 K of 402.1 cSt and a viscosity index of 149.3. The PAO 40 sample was characterized by FTIR (Fig. 2), showing: a weak peak at 720 cm^{-1} which can be assigned to alkyl chains (C-C), a peak at 1465 cm^{-1} due to the carbon–hydrogen (C–H) bending, two strong peaks at 2920 and 2870 cm^{-1} which can be assigned to the C-H stretching [25-27], without any evidence of the signals ascribed for C-C double bonds.

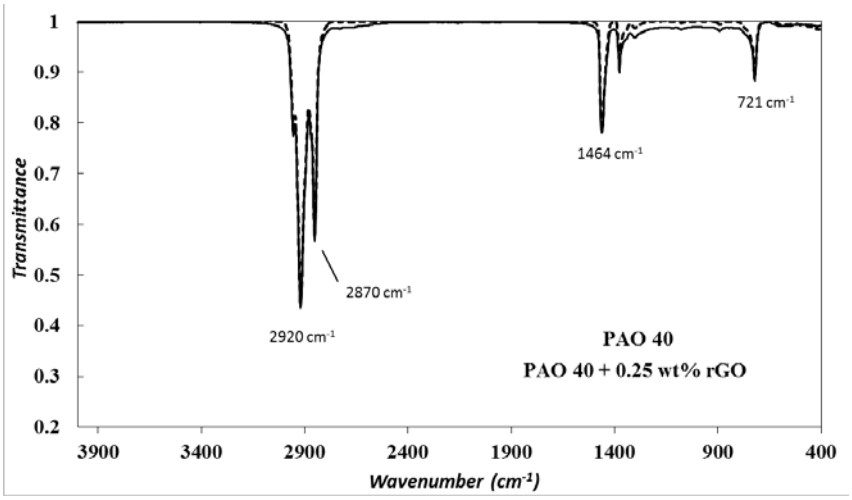

Fig. 2. FTIR spectra of PAO 40 (-) and 0.25 wt% rGO nanodispersion (--).

In order to know if there is a chemical bond between the molecules of the base oil (TMPTO) and the rGO nanopowders, we have compared the FTIR spectra of the neat oil and the nanodispersion with a 0.25 wt% in rGO (Fig. 1). As can be observed, there are no significant changes, indicating the lack of covalent bonds between the TMPTO oil and the rGO nanosheets, thus suggesting that the interactions between rGO and the oil have only physical nature. Similar results were obtained for the rGO nanodispersion in PAO 40 from the comparison of their FTIR spectra (Fig. 2).

2.1.1. Synthesis of rGO

Reduced graphene oxide powders were synthesized following a reported procedure from Li *et al.*[15], but using as starting material graphene oxide monolayer powder (GO) supplied by Nanoninnova Technologies (Spain). GO powders (1.0 g) were mixed with KOH (1.0 g) and ethanol (4.0 mL). After that, this mixture was crushed with a mortar until a viscous black paste was formed. Subsequently, under inert atmosphere of Argon, a thermal treatment was carried out in a tube furnace heating it with a temperature ramp of 5ºC per minute until reaching the desired temperature of 700 °C and keeping at this temperature for additional 4 h. Through this treatment, we assume that GO powders were reduced to rGO sheets. Afterwards, the powder was washed several times with deionized water (3x3 mL) in order to remove residual KOH and

other impurities from the starting GO. Then, the obtained powder was dried at 80 °C for 4 h. The resulting dry powder was crushed in a mortar to reduce the particle size, yielding rGO powders (0.52 g).

2.2. Morphological and Structural Characterization

Both GO and rGO nanopowders were characterized by scanning electron microscopy (SEM) in order to evaluate their morphology and size, and observe the changes occurred in the GO nanosheets after the chemical treatment. SEM micrographs (Fig. 3) were acquired with a Zeiss Ultraplus Field Emission Scanning Electron Microscope, FESEM. High-resolution SEM images show that the rGO sheets are partially exfoliated (Fig. 3), compared to GO nanosheets.

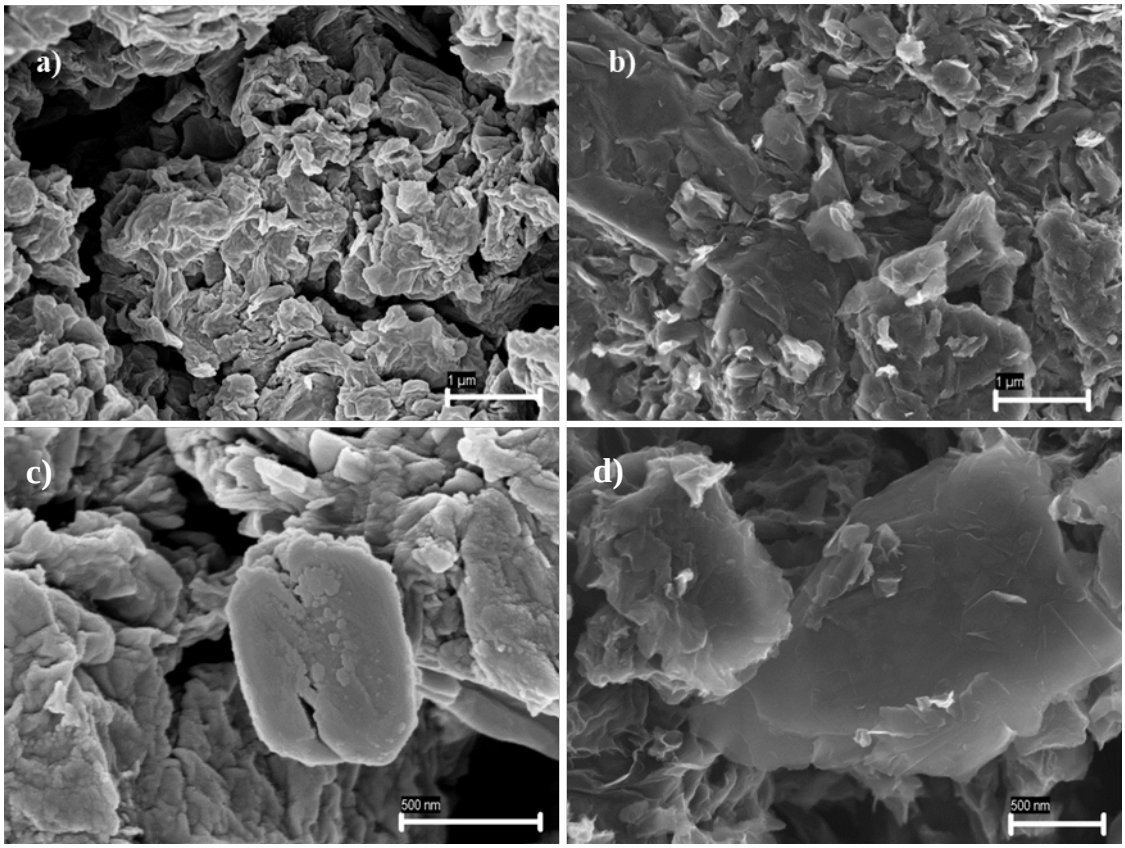

Fig. 3. SEM images of GO (a,c) and rGO (b,d) powders.

In order to characterize rGO and GO, Raman spectroscopy was conducted for both nanopowders. This technique is a powerful tool to analyze the oxygen content of graphitic materials [28]. Both Raman spectra present two bands around 1340 and 1580 cm^{-1} (Fig. 4), which are assigned to the D- and G-bands of carbon [15,29,30]. The D-band is associated with the structural defects or partially disordered structures of graphene oxide, while the G-band is due to the bond stretching of all pairs of sp^2 atoms in both rings and chains of graphene oxide [31]. For GO powders, the ratio of intensities, I_D/I_G, between the two bands is close to unity, namely 0.9. Nevertheless, the Raman spectrum of the rGO nanosheets shows a more intense D-band, with a ratio of intensities (I_D/I_G) of 1.1 [15,29]. The ratio increase indicates a decrease in the average size of the sp^2 domains upon reduction of GO, and it can be interpreted only if additional smaller graphitic domains were originated, apart from those present on the GO before reduction [15,32].

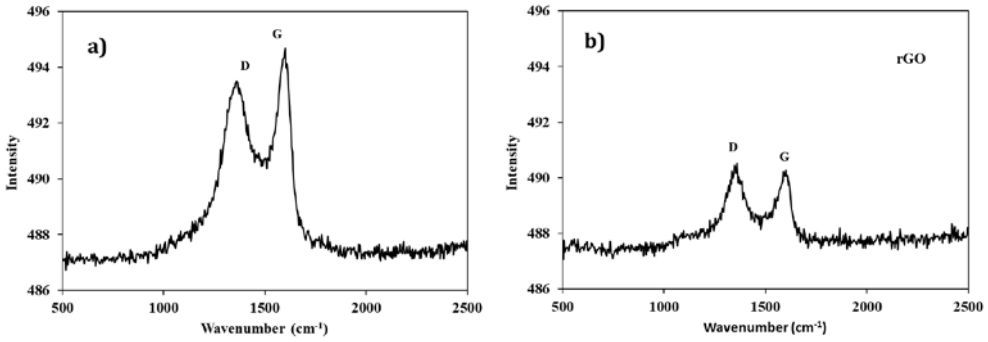

Fig. 4. Raman spectra of (a) GO and (b) rGO.

In addition, rGO powders were characterized by X-ray photoelectron spectroscopy (XPS) with the aim of obtaining quantitative results in relation with the GO reduction. The obtained C 1s spectra for GO and rGO are presented in Figs S1 and S2 of the Supplementary Information, while the elemental composition of both nanopowders are presented in Table 1. The C/O atomic ratio for GO nanopowders is 2.05, being the total area of the bands relative to oxygenated groups (C=O: 287.4 eV, and O-C=O: 288.8 eV) bigger than the area of the band associated with C-C/C=C carbons (285.4 eV) (Fig. S1); these results confirm that our starting material (GO) has

an important number of oxygen atoms. After the thermal treatment with KOH, the atomic ratio C/O increases to 13.29, hence most of the oxygen atoms (79 %) were removed (Table 1). Accordingly, the C 1s XPS spectrum of rGO shows a strong C-C/C=C band (big area) and weak bands associated to oxygenated groups (Fig. S1), confirming the successful reduction of GO.

Table 1

Elemental composition of both nanopowders.

Sample	C	O	K	Ratio C/O
GO	66.67	32.52	0.82	2.05
rGO	91.55	6.89	1.56	13.29

FTIR spectroscopy was also employed to characterize rGO powders (Fig. 5). The GO spectrum (Fig. 5a) exhibits strong vibration bands at: 3418 cm^{-1} corresponding to O−H stretch hydroxyl and phenolic groups, 1735 cm^{-1} attributed to a C=O stretch of carboxyl and carbonyl groups, 1625 cm^{-1} (bending modes of water molecules and C=C stretch), 1355 cm^{-1} (O−H bending), 1240 cm^{-1} (C−O stretch to phenols, ether, and epoxy groups) and 1066 cm^{-1} (C−O stretch correspond to hydroxyl groups) [17,33]. These results show the presence in GO of oxygen functional groups such as carboxyl, hydroxyl, epoxy, etc. linked to the graphene structure. In comparison, the FTIR spectrum of rGO shows the lack of all this bands (Fig 5b), evidencing the success of the thermal treatment removing most of these oxygen functionalities including the carboxylic groups.

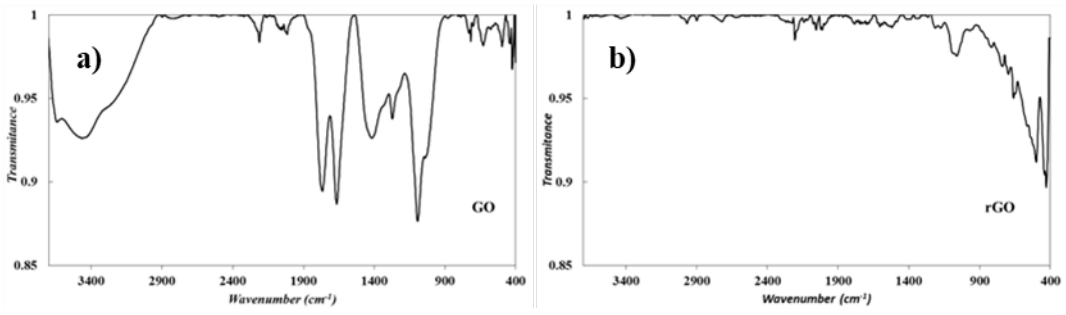

Fig. 5. FTIR spectra of (a) GO and (b) rGO.

2.3. Preparation of the dispersions

Nanolubricants were prepared with different concentrations of rGO (0.05, 0.10, 0.25 and 0.50 wt%) in the base oil, TMPTO or PAO 40. In this work, a two-step procedure was utilized to prepare the nanodispersions [12]. First, rGO dry powder was blended with the base oil; for this step a Sartorius balance (model MC 210P) with a readability of 0.01 mg was used in order to determine the concentration. Then, homogenization of the system was carried out with a Fisherbrand ultrasonic bath, in a continuous shaking mode during 4 hours with an effective power of 180W and a fixed sonication frequency of 37 kHz.

	0 h	24 h	48 h	120 h	148 h	244 h
99.75 wt% TMPTO + 0.25 wt% GO						
99.75wt% TMPTO + 0.25 wt% rGO						
99.75 wt% PAO 40 + 0.25 wt% GO						
99.75wt% PAO 40 + 0.25 wt% rGO						

Fig. 6. Photographs used for assigning the stability of the nanodispersions.

The stability of the nanolubricants was, in a first step, studied by visual observation. This analysis was performed also for the nanodispersion containing GO in order to determine the increase in stability against the sedimentation of rGO nanosheets with respect to the GO ones. The chosen concentration was 0.25% because it is intermediate in the range of the prepared nanodispersions. For GO nanodispersions the first signs of sedimentation appeared 24 h after sonication (Fig. 6), whereas for rGO dispersions no signs of sedimentation were observed for the first 240 h for both neat oils. This time is much longer than the necessary to carry out the tribological studies (about four hours).

Refractometry was the second analysis technique used to check the increase in stability for the rGO nanopowders. The evolution of the refractive index with time it is depicted in Figure 7. The increase in the refractive indexes is lower for the nanodispersions containing rGO than for those containing GO, regardless the base oil used, TMPTO (Fig. 7a) or PAO 40 (Fig. 7b). These results show the great stability improvement for the nanodispersions containing rGO in comparison to those with GO.

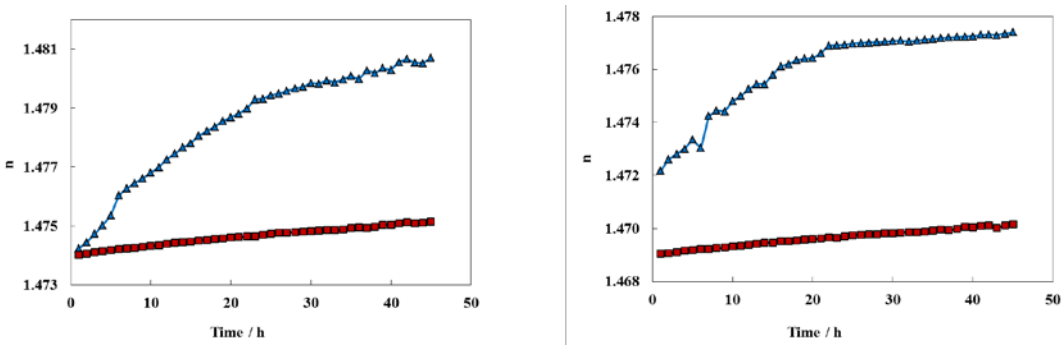

Fig. 7. Temporal evolution of the refractive index, *n*: a) 0.05 wt% GO (▲) and 0.05 wt% rGO (■) in TMPTO b) 0.05 wt% GO (▲) and 0.05 wt% rGO (■) in PAO 40.

Dynamic light scattering has also been used (Zetasizer Nano ZS DLS) in order to check the stability of nanodispersions, together with obtaining the apparent average size of dispersed nanosheets in the two base oils. We refer to apparent average size because this technique has been designed to study spherical particles whereas the present nanoadditives are flake-like shaped. More details were indicated previously [25]. For TMPTO and PAO 40 nanofluids

apparent average sizes of around 630 nm and 60 nm were found respectively, at the same concentration of nanodispersion (0.25wt% rGO) for both base oils. The smaller apparent average sizes found for PAO 40 rGO nanodispersion may be due to lower probability of collision of the nanoparticles in the more viscous fluid) because a lower Brownian motion [34]. DLS data (Fig. 8) reveal that both nanolubricants do not present high sedimentation at the initial stage (70 h since sonication), being this period of time smaller than the necessary to carry out the tribological measurements.

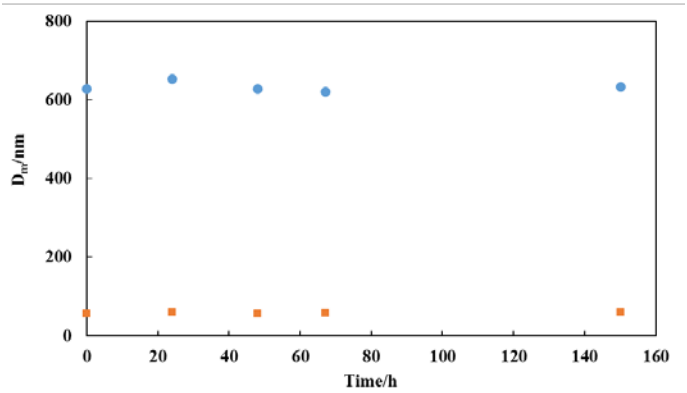

Fig. 8. Apparent average particle size, D_m, obtained by DLS for nanodispersions at 0.25wt% rGO concentration in: TMPTO (●) and PAO 40 (■).

2.4. Tribological Tests

With the aim of determining the friction coefficients, rotational friction tests were carried out using a CSM Standard tribometer in a ball-on-disk configuration. Thus, chrome steel balls AISI 52100/535A99 (diameter: 6 mm; roughness <0.05 μm, hardness: 58-66 Rockwell "C" Scale) were run against AISI 52100/535A99 circular stainless steel plates (diameter: 10 mm; surface finish <0.02 μm Ra; hardness: 190-210 Hv30). Before starting a test, both the plates and the balls were cleaned with hexane and dried in hot air. After that, these specimens were lubricated with three drops of the lubricant under study. Tests were conducted under a normal load of 20 N that corresponds to a maximum contact pressure of 1.79 GPa. At least three replicates were performed for each sample at a trajectory radius of 3 mm, speed of 0.08 $m \cdot s^{-1}$ and a sliding

distance of 340 m. After performing the experiments, both the plates and the balls were washed with hexane.

Wear in plates was evaluated in terms of the width, depth and cross-section area of the wear track as well as the roughness of the worn surface by means of a 3D Optical Profiler Sensofar S Neox. Although the circular wear scars on the plates seem quite uniform, for each sample the width and depth below the unworn surface were measured in three different zones, in order to obtain representative average values. To perform these measurements, the confocal mode was used to analyze both the balls and the plates with a 10X objective. A stitching operation was used in order to get the full images of the wear scar.

3. Results and Discussion

3.1. Tribological Behavior

Friction coefficients, μ, obtained for the nanolubricants with 0.05, 0.10, 0.25 and 0.50 wt% of rGO, in TMPTO and PAO40 are reported in Table 2 and shown in Figs. 9 and 10, respectively. It can be clearly observed that for all the nanodispersions with TMPTO, the coefficient of friction is reduced with respect to that obtained with the base oil, obtaining the greatest friction reduction for the nanolubricant with a concentration of 0.25 wt%. Thus, a friction coefficient of 0.0721 was obtained for this optimal concentration against 0.0904 for the neat TMPTO oil, as can be seen in Table 2. On the other hand, for all nanolubricants prepared with PAO 40, the friction coefficient was also reduced with respect to the base oil, obtaining the best friction behavior again for the nanolubricant of 0.25 wt% rGO. The relative reduction in the friction coefficient, $100\left(\left(\mu_{oil} - \mu_{dispersion}\right)/\mu_{oil}\right)$, calculated for the best antifriction behavior, 0.25 wt% rGO dispersion, is around 20% for TMPTO and 24% for the nanolubricant based on PAO 40.

Table 2

Mean values of the friction coefficient, μ, and of the width, WTW, depth, WTD, and cross-section area of the wear track and their respective standard deviations for all nanolubricants.

wt%	μ	σ	WTW/μm	σ/μm	WTD/μm	σ/μm	Area/μm^2	σ/μm^2
			TMPTO + rGO					
0	0.0904	0.0013	361	9	2.17	0.05	447	20
0.05	0.0818	0.0009	*285*	12	2.12	0.05	325	18
0.10	0.0802	0.0010	299	8	2.09	0.04	334	17
0.25	0.0721	0.0016	274	6	2.02	0.04	303	14
0.50	0.0837	0.0022	*299*	8	2.29	0.06	340	18
			PAO40 + rGO					
0	0.0944	0.0010	287	8	1.26	0.11	302	27
0.05	0.0795	0.0017	284	18	1.32	0.07	288	24
0.10	0.0747	0.0002	278	10	1.18	0.14	280	27
0.25	0.0715	0.0012	276	7	1.05	0.03	280	11
0.50	0.0804	0.0011	298	7	1.32	0.08	311	14

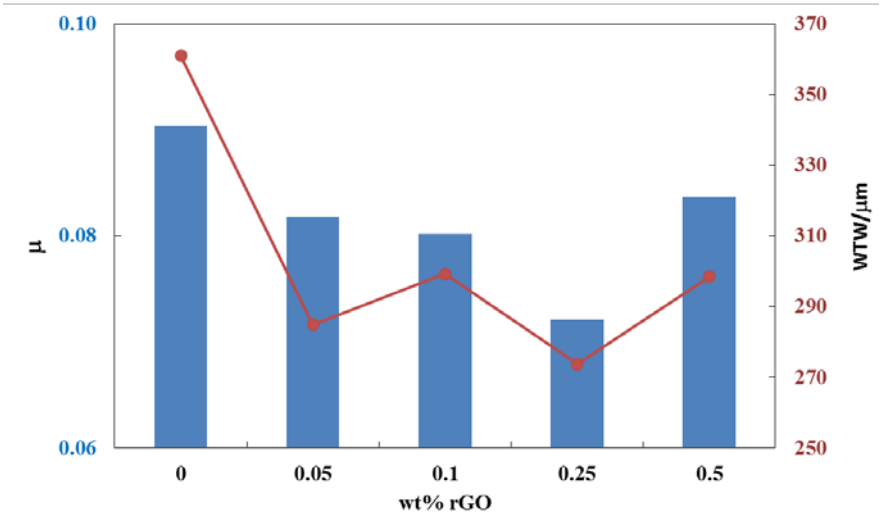

Fig. 9. Friction coefficient, μ, (■) and wear track width, WTW, (●) obtained with the base oil TMPTO and with the rGO nanolubricants.

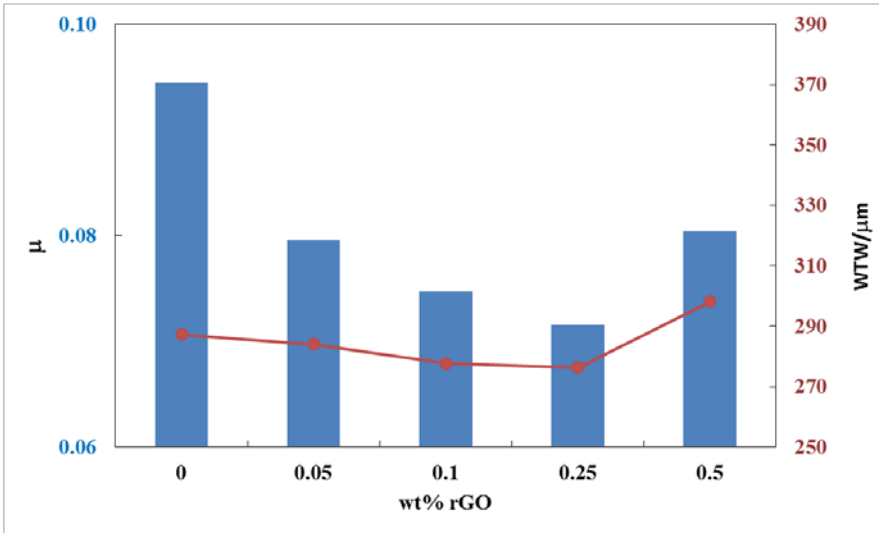

Fig.10. Friction coefficient, μ, (■) and wear track width, WTW, (●) obtained with the base oil PAO 40 and with the rGO nanolubricants.

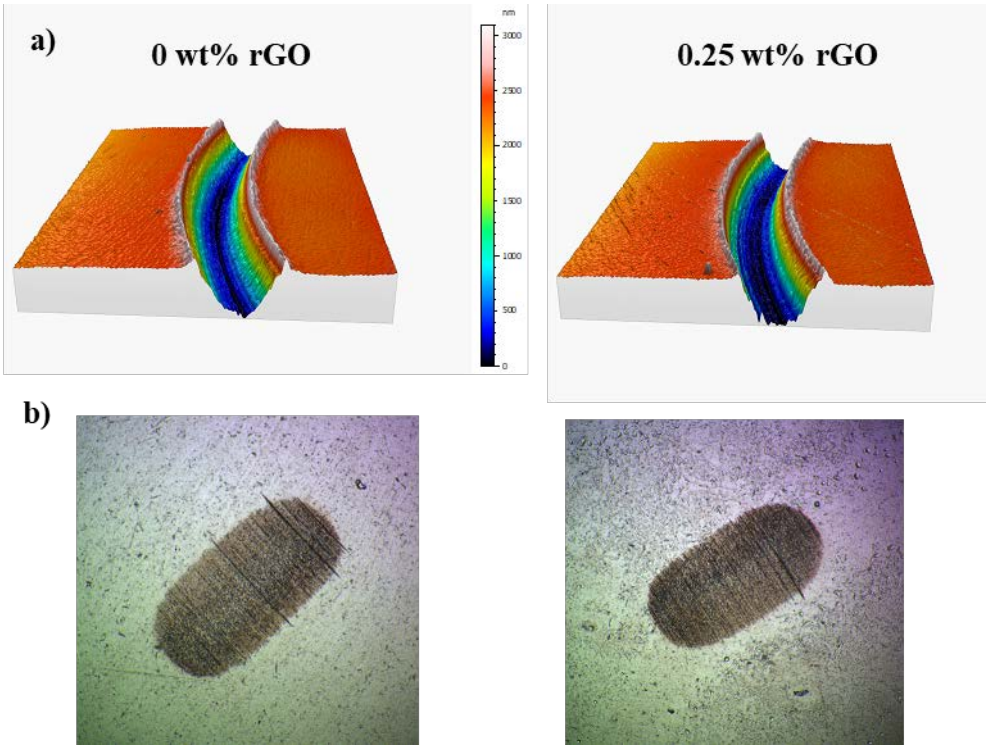

Fig. 11. (a) 3D profile (10x) of the wear tracks on the plates and (b) images of the wear surface of the balls on the contact lubricated with neat TMPTO (left) and with the nanolubricant containing a 0.25 wt% of rGO (right).

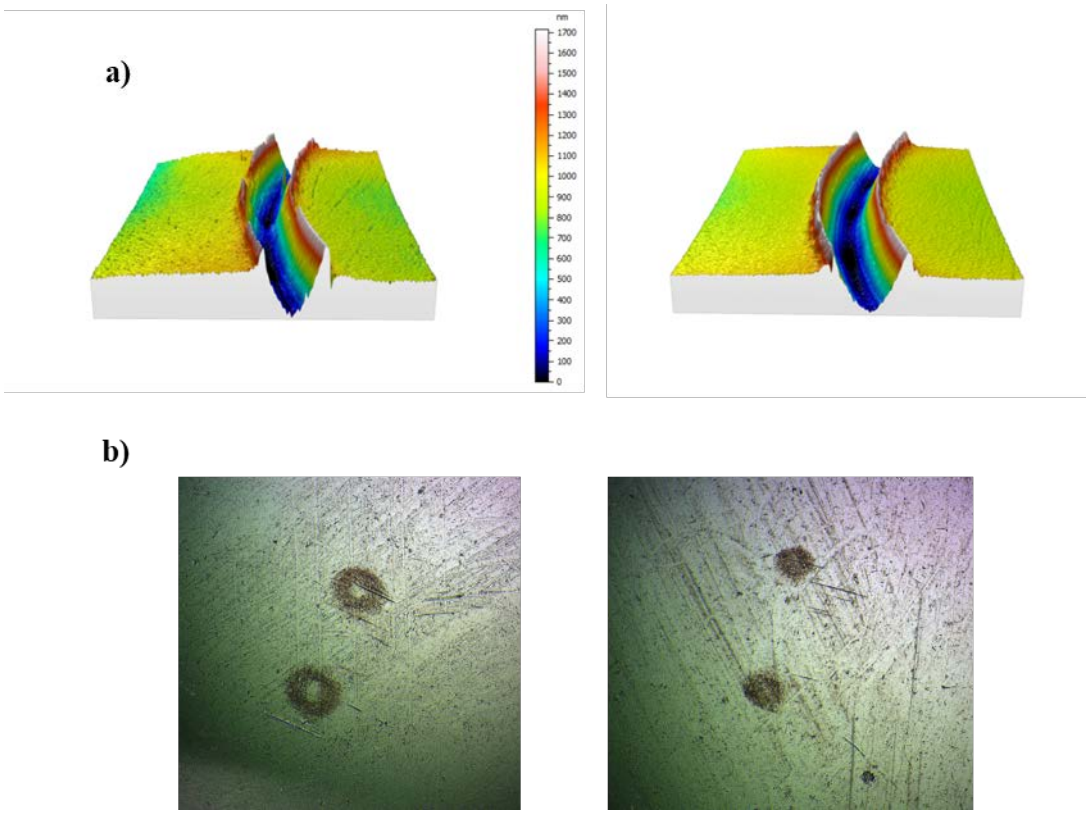

Fig. 12. (a) 3D profile (10x) of the wear tracks on the plates and (b) images of the wear surface of the balls on the contact lubricated with neat PAO 40 (left) and with the nanolubricant containing a 0.25 wt% of rGO (right).

The wear tracks obtained for the base oils and for the 0.25 wt% rGO in both TMPTO and PAO 40 are shown in Fig. 11 and Fig. 12, respectively. In the same figures the wear marks belonging to the balls as well as the wear profiles produced in the plates can be also observed. The wear on the plates was analyzed in terms of not only the width, but also the depth and cross-section area both below the unworn surface of the scar. In Figs. 13 and 14 the cross-section profiles of the groves on the plate lubricated with neat TMPTO or PAO 40, respectively, and their dispersions containing a 0.25 wt% of rGO. As can be seen in Table 2, WTW and cross-section area are reduced for all the nano-lubricants studied with respect to the neat base oil TMPTO, obtaining a maximum wear reduction for the concentration of 0.25 wt% rGO (24 % and 32 % respectively), while the depth slightly varies for the different nanolubricants. A good relationship between friction and wear was found, since for the same concentration of nanolubricant, 0.25 wt% rGO, the best antifriction-antiwear behavior has been obtained. Furthermore, for the PAO 40

nanolubricants, as can be seen in Table 2, the wear track width and cross-section area hardly vary for the different concentrations of rGO whereas the depth decreases down to 17 % for the 0.25 wt% rGO dispersion. For this last concentration also minimum values for WTW and the cross-section area were found (respectively 4 % and 7 % of decrease in comparison with the neat PAO 40). Thus, the antiwear capability of PAO 40 can be only slightly improved by the presence of this nanoadditive. On the other hand, wear obtained with the nano-lubricants based on PAO 40 are lower than those of dispersions based on TMPTO.

The antiwear capability of the nanolubricants was confirmed comparing the roughness of the worn surfaces obtained with both 0.25 rGO wt% nanolubricants with those of the two base oils (TMPTO and PAO 40). The roughness parameter *Ra* was determined accordingly to the standard ISO 4287 applying a Gaussian filter with a long wavelength cut-off of 0.08 mm. A *Ra* value of 76 nm was obtained for the worn surface lubricated with TMPTO whereas for the scar corresponding to the 0.25 wt% in rGO nanolubricant *Ra* was found to be only 24 nm; indicating that the nano-dispersion produces a smoother surface compared to those of the TMPTO base oil; whereas for the PAO 40 nanolubricant (13 nm) the reduction of roughness compared with the base oil (14 nm) is not significant.

Good antifriction and antiwear capabilities were found by Li *et al.* [15] with rGO nanopowders as additives of other polyalphaolefin (PAO 6). These authors attribute these good results to two effects: the patching effect and the formation of a protective boundary film physically adsorbed on the rubbing surfaces. Several authors have concluded that the key factor for the reduction in friction and wear is precisely the formation of these adsorbed graphene/graphite tribofilms in the contact [4,13,17,35].

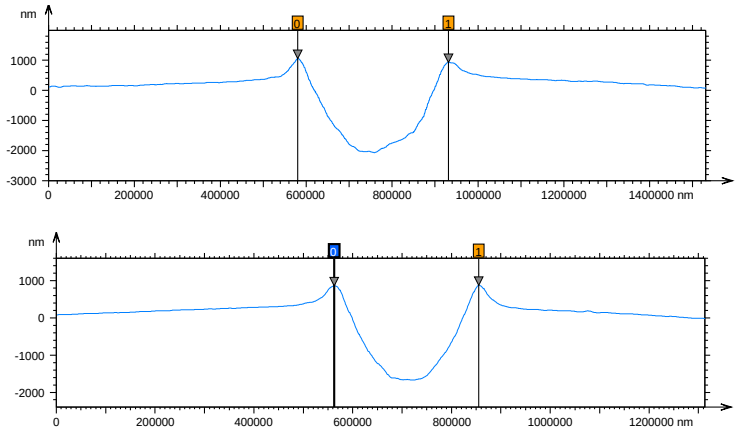

Fig. 13. Cross section profiles of the wear tracks on the plate lubricated with neat TMPTO (top) and with the nanolubricant containing a 0.25 wt% of rGO (bottom).

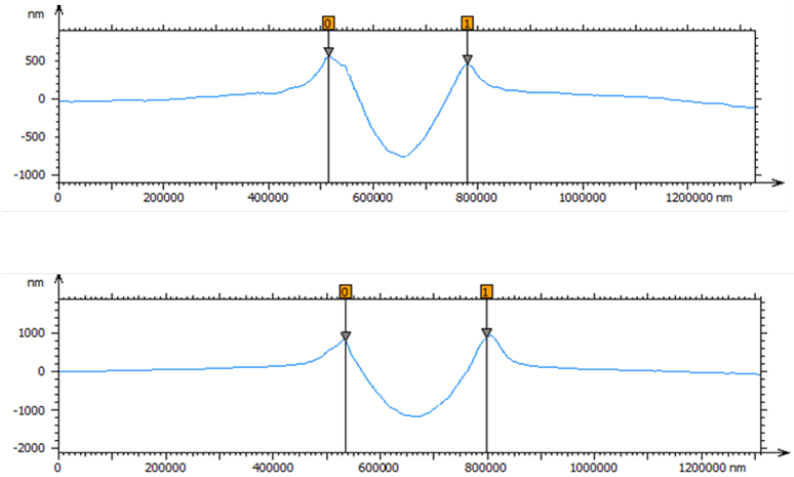

Fig. 14. Cross section profiles of the wear tracks on the plate lubricated with neat PAO 40 (top) and with the nanolubricant containing a 0.25 wt% of rGO (bottom).

In order to confirm these mechanisms of protection against wear, the wear scars of all nanolubricants produced on the plates were analyzed by Raman spectroscopy. For this study, after the tribological tests, the plates were cleaned using an ultrasonic technique in an acetone bath, in order to remove the residual lubricant in the wear scar. As it can be observed in the Raman spectrum of the worn surface (Fig. 15) the characteristic D and the G-bands (around 1340 and 1580 cm^{-1}, respectively) of rGO nanopowders appear, confirming a physical adsorption of the rGO nanopowders in the worn area, forming a boundary film protection [7]. Other feature of this nanoadditive is its lamellar structure, which offers low shear stress and prevents interaction at the rubbing interfaces.

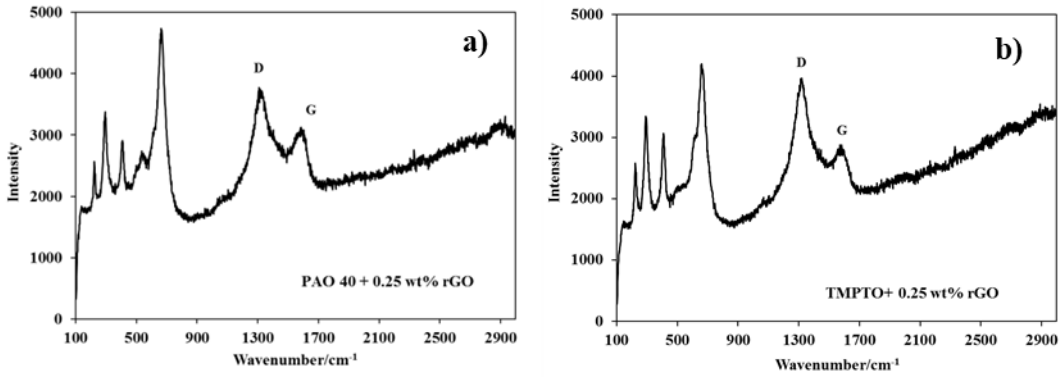

Fig. 15. Raman spectra of wear scar on the plates previously lubricated with (a) a dispersion of PAO 40 with 0.25 wt% of rGO and (b) a dispersion of TMPTO with 0.25 wt% of rGO.

The tests performed in the present work correspond to the boundary lubrication regime. It is in this regime where the presence of nanoparticles can have a beneficial effect. Comparing the friction coefficient and wear obtained for the different concentrations of nanoadditives tested, an optimal concentration of 0.25 wt % of nanoparticles was found for both oils. At lower concentrations, the quantity of nanoparticles is not sufficient to prevent wear, being the behavior govern by the base oil; when the concentration is too high, nanoparticles tend to agglomerate, thus reducing the suspension stability, and the formation of large size aggregates which scratch the surface under loading [13,16,36].

4. Conclusions

In this work the following features were achieved:

1. Reduced graphene oxide nanopowders, rGO, with only 7% of Oxygen content have been synthesized.
2. Dispersions of two base oils (TMPTO or PAO 40) with (0.05, 0.10, 0.25 and 0.50) wt% of GO or rGO were prepared showing that through chemical modification of GO, a greater stability of the nanodispersions is achieved.
3. The friction coefficient was for all the nanolubricants lower than that obtained with base oils.

4. The wear track widths and the cross-sectional areas obtained with the four nanolubricants based on TMPTO are lower than those corresponding to the neat oil.
5. The minimum wear parameters and the best friction coefficient were obtained for the nanolubricant based on TMPTO additivated with a 0.25 wt% in rGO. Thus, this composition optimizes the antifriction and antiwear capabilities respect to those of the neat oil.
6. The wear track widths and the cross-section areas of nanolubricants based on PAO 40 are similar for all concentrations, obtaining a slightly better behavior for 0.25 wt% rGO.
7. A lower wear is obtained with the nano-lubricants based on PAO 40 than with those of TMPTO.
8. From the Raman spectroscopy in the plates wear tracks, we can conclude that there is physical adsorption of the rGO nanopowders in the friction pairs.

Acknowledgments

It is a pleasure to thank Professor Diego Peña (CIQUS and Departamento de Química Orgánica, University of Santiago de Compostela for kindly allowing the use of his Laboratory for the synthesis of rGO and his continuous advice. We would like to thank Croda and REPSOL for providing our laboratory with the TMPTO and the PAO 40 samples. Authors also acknowledge Nanoinnova Technologies S.L. (www.nanoinnova.com) for providing the Graphene Oxide monolayer powder. This work was supported by both the Spanish Ministry of Economy and Competitiveness and the European Regional Development Fund (ERDF) programme through ENE2014-55489-C2-1-R and ENE2017-86425-C2-2-R projects. Moreover, this work was funded by the Xunta de Galicia (GRC ED431C 2016/001). The three last funders also financed the acquisition of the 3D Optical Profile Sensofar S Neox (UNST15-DE-3156). JMLR acknowledges Xunta de Galicia for a Principia contract. FG is grateful for financial support from the Xunta de Galicia (Centro Singular de Investigación de Galicia accreditation 2016–2019, ED431G/09) and

the European Union (ERDF). Authors would like to thank the use of RIAIDT-USC analytical facilities.

5. References

[1] J. Padgurskas, R. Rukuiza, I. Prosyčevas, R. Kreivaitis, Tribological properties of lubricant additives of Fe, Cu and Co nanoparticles, Tribol. Int. 60 (2013) 224-232.
[2] A.B. Najan, R.R. Navthar, M.J. Gitay, Experimental Investigation of Tribological Properties Using Nanoparticles as Modifiers in Lubricating Oil, IRJET 04 (2017) 1125-1129.
[3] S. Shahnazar, S. Bagheri, S.B.A. Hamid, Enhancing lubricant properties by nanoparticle additives, Int. J. Hydrog. Energy 41 (2016) 3153-3170.
[4] D. Berman, A. Erdemir, A.V. Sumant, Graphene: A new emerging lubricant, Mater. Today Proc. 17 (2014) 31-42.
[5] A.K. Rasheed, M. Khalid, W. Rashmi, T.C.S.M. Gupta, A. Chan, Graphene based nanofluids and nanolubricants – Review of recent developments, Renew. Sust. Energ. Rev. 63 (2016) 346-362.
[6] A.K. Sharma, A.K. Tiwari, A.R. Dixit, R.K. Singh, Investigation into Performance of SiO2 Nanoparticle Based Cutting Fluid in Machining Process, Mater. Today Proc. 4 (2017) 133-141.
[7] M. Farsadi, S. Bagheri, N.A. Ismail, Nanocomposite of functionalized graphene and molybdenum disulfide as friction modifier additive for lubricant, J. Mol. Liq. 244 (2017) 304-308.
[8] M.S. Dresselhaus, A. Jorio, R.Saito, Characterizing Graphene, Graphite, and Carbon Nanotubes by Raman Spectroscopy, Annu. Rev. Condens. Matter Phys. 1 (2010) 89-108.
[9] V. Eswaraiah, V. Sankaranarayanan, S. Ramaprabhu, Graphene-Based Engine Oil Nanofluids for Tribological Applications, ACS Appl. Mater. Interfaces 3 (2011) 4221-4227.
[10] D. Berman, A. Erdemir, A.V. Sumant, Few layer graphene to reduce wear and friction on sliding steel surfaces, Carbon 54 (2013) 454-459.
[11] S. Choudhary, H.P. Mungse, O.P. Khatri, Dispersion of alkylated graphene in organic solvents and its potential for lubrication applications, J. Mater. Chem. 22 (2012) 21032-21039.
[12] S. Kannaiyan, C. Boobalan, A. Umasankaran, A. Ravirajan, S. Sathyan, T. Thomas, Comparison of experimental and calculated thermophysical properties of alumina/cupric oxide hybrid nanofluids, J. Mol. Liq. 244 (2017) 469-477.
[13] B. Gupta, N. Kumar, K. Panda, S. Dash, A.K. Tyagi, Energy efficient reduced graphene oxide additives: Mechanism of effective lubrication and antiwear properties, Sci. Rep. 6 (2016) 18372.
[14] E. Varrla, S. Venkataraman, R. Sundara, Graphene-Based Engine Oil Nanofluids for Tribological Applications, ACS Appl. Mater. Interfaces 3 (2011) 4221-4227.
[15] Y. Li, J. Zhao, C. Tang, Y. He, Y. Wang, J. Chen, J. Mao, Q. Zhou, B. Wang, F. Wei, J. Luo, G. Shi, Highly Exfoliated Reduced Graphite Oxide Powders as Efficient Lubricant Oil Additives, Adv. Mater. Interfaces 3 (2016) 1600700.
[16] B. Schlüter, R. Mülhaupt, A. Kailer, Synthesis and Tribological Characterization of Stable Dispersions of Thermally Reduced Graphite Oxide, Tribol. Lett. 53 (2014) 353-363.
[17] H.P. Mungse, O.P. Khatri, Chemically Functionalized Reduced Graphene Oxide as a Novel Material for Reduction of Friction and Wear, J. Phys. Chem. C 118 (2014) 14394-14402.
[18] H. Kinoshita, Y. Nisina, A.A. Alias, M. Fujii, Tribological properties of monolayer graphene oxide sheets as water-based lubricant additives, Carbon 66 (2014) 720-723.
[19] W. Zhang, M. Zhou, H. Zhu, Y. Tian, K. Wang, J. Wei, F. Ji, X. Li, Z. Li, P. Zhang, D. Wu, Tribological properties of oleic acid-modified graphene as lubricant oil additives, J. Phys. D Appl. Phys. 44 (2011) 205303.

[20] E. Beran, M. Łoś, A. Kmiecik, Influence of thermo-oxidative degradation on the biodegradability of lubricant base oils, J. Synth. Lubr. 25 (2008) 75-83.
[21] I. Otero, E.R. López, M. Reichelt, M. Villanueva, J. Salgado, J. Fernández, Ionic Liquids Based on Phosphonium Cations As Neat Lubricants or Lubricant Additives for a Steel/Steel Contact, ACS Appl. Mater. Interfaces 6 (2014) 13115-13128.
[22] Y. Wu, W. Li, X. Wang, Synthesis and properties of trimethylolpropane trioleate as lubricating base oil, Lubr. Sci. 27 (2015) 369-379.
[23] R. Benda, J. Bullen, A. Plomer, Synthetics basics: Polyalphaolefins — base fluids for high-performance lubricants, J. Synth. Lubr. 13 (1996) 41-57.
[24] L.R. Rudnick, Polyalphaolefins in: L.R. Rudnick, (Ed.), Synthetics, Mineral Oils, and Bio-Based Lubricants: Chemistry and Technology, CRC Press, 2013.
[25] J.M. Liñeira del Río, M.J.G. Guimarey, M.J.P. Comuñas, E.R. López, A. Amigo, J. Fernández, Thermophysical and tribological properties of dispersions based on graphene and a trimethylolpropane trioleate oil, J. Mol. Liquids 268 (2018) 854-866.
[26] X. Zhang, S. Wan, J. Pu, L. Wang, X. Liu, Highly hydrophobic and adhesive performance of graphene films, J. Mater. Chem. 21 (2011) 12251-12258.
[27] V. Adam, F. Jacek, Chromatographic and non-chromatographic characterization of poly-α-olefins, J. Synth. Lubr. 24 (2007) 91-100.
[28] E.K. Goharshadi, Z. Niyazi, M. Shafaee, M.B. Moghaddam, R. Ludwig, M. Namayandeh-Jorabchi, Transport properties of graphene quantum dots in glycerol and distilled water, J. Mol. Liq. 241 (2017) 831-838.
[29] J. Chen, Y. Zhang, M. Zhang, B. Yao, Y. Li, L. Huang, C. Li, G. Shi, Water-enhanced oxidation of graphite to graphene oxide with controlled species of oxygenated groups, Chem. Sci. 7 (2016) 1874-1881.
[30] S. Ye, B. Chen, J. Feng, Fracture Mechanism and Toughness Optimization of Macroscopic Thick Graphene Oxide Film, Sci. Rep. 5 (2015) 13102.
[31] A. Ferrari, Raman Spectroscopy of Graphene and Graphite: Disorder, Electron-Phonon Coupling, Doping and Nonadiabatic Effects, Solid State Commun. 143 (2007) 47-57.
[32] S. Stankovich, D.A. Dikin, R.D. Piner, K.A. Kohlhaas, A. Kleinhammes, Y. Jia, Y. Wu, S.T. Nguyen, R.S. Ruoff, Synthesis of graphene-based nanosheets via chemical reduction of exfoliated graphite oxide, Carbon 45 (2007) 1558-1565.
[33] M. Acik, G. Lee, C. Mattevi, A. Pirkle, R.M. Wallace, M. Chhowalla, K. Cho, Y. Chabal, The Role of Oxygen during Thermal Reduction of Graphene Oxide Studied by Infrared Absorption Spectroscopy, J. Phys. Chem. C 115 (2011) 19761-19781.
[34] M.J.G. Guimarey, M.R. Salgado, M.J.P. Comuñas, E.R. López, A. Amigo, D. Cabaleiro, L. Lugo, J. Fernández, Effect of ZrO2 nanoparticles on thermophysical and rheological properties of three synthetic oils, J. Mol. Liq. 262 (2018) 126-138.
[35] H.P. Mungse, N. Kumar, O.P. Khatri, Synthesis, dispersion and lubrication potential of basal plane functionalized alkylated graphene nanosheets, RSC Adv. 5 (2015) 25565-25571.
[36] V. Zin, S. Barison, F. Agresti, L. Colla, C. Pagura, M. Fabrizio, Improved tribological and thermal properties of lubricants by graphene based nano-additives, RSC Adv. 6 (2016) 59477-59486.